Motion-Induction Compensation to Mitigate Sub-Synchronous Oscillation in Wind Farms

Yunjie Gu, *Member, IEEE*, Jiao Liu, Timothy C. Green, *Fellow, IEEE*,
Wuhua Li, *Member, IEEE*, Xiangning He, *Fellow, IEEE*

***Abstract*—This paper presents a comprehensive solution to mitigate the sub-synchronous oscillation (SSO) in wind farms connected to series-compensated transmission lines. The concept of motion-induction amplification (MIA) is introduced to reinterpret the physical root cause of the negative resistance in doubly-fed induction generators (DFIGs). Based on this new interpretation, a novel control scheme called motion-induction compensation (MIC) is proposed to counteract the MIA effect. The MIC control eliminates the negative resistance in DFIGs across the entire frequency range, and makes the Type-III (DFIG) generator behave like a Type-IV generator in dynamics. The proposed solution provides wide-range SSO damping and also shows excellent robustness against model and measurement errors.**

***Index Terms*—Sub-synchronous oscillation, wind farm, DFIG, series compensation, motion-induction compensation**

I. Introduction

Type-III wind turbines have become the mainstream technology for on-shore wind power generation, as they provide a good balance between cost, reliability, and controllability [1]–[5]. However, the doubly-fed induction generators (DFIGs) in Type-III turbines may induce sub-synchronous oscillation (SSO) on series-compensated lines, which may cause tripping of wind farms, transmission lines and even gas-turbine generators nearby, posing a threat to power system stability [6]–[9]. Many accidents have been reported worldwide and both academia and industry are looking for a comprehensive solution to mitigate this challenge [10], [11].

The DFIG SSO is attributed to the induction generator effect which leads to negative resistance and excites the LC resonance on series-compensated lines [12]–[14]. This effect is common in both synchronous generators (with amortisseur windings) and induction generators, but the control actions on DFIGs vastly increase the negative resistance and hence the possibility of oscillation. Therefore, the DFIG SSO is categorized as sub-synchronous control interaction (SSCI) beyond the conventional sub-synchronous resonance (SSR). [15]

Yunjie Gu and Timothy C. Green are with the Department of Electrical and Electronic Engineering, Imperial College London. Jiao Liu is with GE Renewable Energy. Wuhua Li and Xiangning He are with the College of Electrical Engineering, Zhejiang University. E-mail: yunjie.gu@imperial.ac.uk; t.green@imperial.ac.uk; jiao.liu1@ge.com; woohualee@zju.edu.cn; hxn@zju.edu.cn.

This work was supported by the Engineering and Physical Sciences Research Council of UK (EP/S000909/1) and by GE Renewable Energy. The Matlab/Simulink models used in generating the results in this paper are available from the website https://spiral.imperial.ac.uk.

Reducing the rotor-side current control gain is taken as an easy method to mitigate the risk of DFIG SSO [16], but this comes at the expense of worsened current control, meaning poorer power quality and slower dynamic response. Moreover, the negative resistance is only attenuated, not entirely removed, so the risk of SSO still exists. Instead of naive gain reduction, a sub-synchronous notch filter can be inserted into the current control loop to reduce the current control gain only at sub-synchronous frequency [17]. This helps to alleviate the negative impact on power quality and dynamic response and improves damping performance.

Alternatively, supplementary damping control has been proposed to mitigate SSO without changing the original current controller structure. The supplementary controller takes feedback from sensors [18], [19] or state observers [20] and generates auxiliary damping signals injected at various points in either the rotor-side or grid-side controller. The optimal selection of feedback signals and damping injection points was investigated in [21], and it was pointed out that feedback of the voltage of series capacitor is inevitably needed to ensure effective damping of SSO without destabilizing other modes. Series capacitor voltage cannot be measured locally but can be estimated indirectly via transmission line current [21], [22]. However, such an estimation relies on the prior knowledge of the value of the series capacitance, which might not be disclosed and is also liable to vary in real time due to changes of network topology and control actions of the transmission system operator (TSO). The lack of an accurate value may lead to inaccurate estimation of the capacitor voltage which will compromise the effectiveness of damping. As a result, supplementary damping control only partly solves the problem in some practical cases and SSO accidents still occur occasionally [23].

This paper introduces a new approach to providing SSO damping which is significantly different to supplementary damping control. Instead of working on the resonance of series-compensated lines, the proposed method works on the intrinsic dynamics of DFIGs so as to eliminate the negative resistance that can arise, and thereby provides robust SSO damping which is insensitive to the changes in the parameters of series-compensated lines. A new concept called *motion-induction amplification* (MIA) is introduced that is a reinterpretation of the physical root cause of DFIG negative resistance. It is shown that the composition of the motional and induced electromotive force (EMF) on the rotor winding forms an equivalent amplifier. This amplifier has negative gain for frequencies between zero and the rotor frequency and therefore

maps positive resistance on the rotor side to negative resistance on the stator side. In the light of this interpretation, the negative resistance can be eliminated by counteracting the MIA effect via control action. Thus is derived a new SSO damping control scheme which has been named *motion-induction compensation* (MIC). MIC renders the small-signal behavior of a Type-III turbine identical to that of a Type-IV turbine and therefore eliminates the possibility of SSO with series-compensated lines regardless of compensation parameters.

The paper is organized as follows. The principle of MIA is explained in Section II, based on which the MIC schemes are derived in Section III. Section IV demonstrates the robustness of MIC against model and measurement errors. Section V demonstrate the advantage of the proposed solution with a series of simulation tests. Section VI concludes the paper.

II. Motion-Induction Amplification

It has been well-accepted that SSO in DFIGs is to a great extent excited by the inner current loop of the rotor-side converter (RSC) [24]. The outer control loops, including the phase-locked loop, dc-link control, voltage-var(reactive power) control, and torque-speed control are usually designed to have lower bandwidth (<10Hz) than the SSO frequency (>20Hz) and therefore have smaller if not negligible possibility of participating in the SSO. The grid-side converter (GSC) may also introduce negative resistance but this could be avoided in sub-synchronous frequency provided that the outer control loops are properly designed [25], [26]. Wind turbines usually have a very large inertia and stiff shaft systems so the rotor speed can be assumed constant in SSO analysis. Based on these considerations, this paper is focused on the inner current loop of the RSC and its interaction with the series-compensated line via the flux dynamics of a DFIG. A comprehensive DFIG model including all control loops can be found in [13], which turns out to have similar results to this paper and justifies the assumption above.

Focusing on RSC inner loops enables a more intuitive insight into the physics of DFIG SSO and sheds light on counteracting control schemes to mitigate SSO, which is invisible from prior-art models. It allows us to investigate a DFIG from the rotor's perspective and unfold the internal structure of rotor flux dynamics. From this perspective, it is found that there is an intrinsic amplifier on the rotor side formed by the combination of motional and induced EMF, which is named motion-induction amplification (MIA). MIA plays a central role throughout this paper and is illustrated in detail below.

Although a DFIG is usually controlled in the synchronous frame (dq), we choose to model it in the stationary frame ($\alpha\beta$) here to reveal the combination structure of the rotor EMF. Frame transformation between dq and $\alpha\beta$ are conducted when necessary, and the complex signal notation is used to represent frame transformation as frequency shifting [27]–[31]. In the stationary frame, the electrical dynamics of a DFIG can be described by

$$\text{state equation:} \begin{cases} \dot{\psi}_s = v_s - i_s R_s \\ \dot{\psi}_r = v_r + j\omega_r \psi_r - i_r R_r \end{cases} \\ \text{flux equation:} \begin{cases} \psi_s = L_m \cdot (i_s + i_r) + L_{\sigma s} \cdot i_s \\ \psi_r = L_m \cdot (i_s + i_r) + L_{\sigma r} \cdot i_r \end{cases} \tag{1}$$

in which v, i, and ψ are voltage, current, and flux vectors written as complex numbers, and the subscript $_s$ and $_r$ stand for stator and rotor respectively. R_s and R_r are winding resistance, $L_{\sigma s}$, $L_{\sigma r}$, and L_m are leakage and mutual inductance, and ω_r is the rotor electrical frequency. We assume ω_r to be constant when analyzing SSO as ω_r changes very slowly due to the high inertia of turbines.

The rotor voltage v_r is governed by the rotor-side converter with closed-loop current control:

$$v_r = Z_{rc} \cdot (i_r^* - i_r) \tag{2}$$

in which Z_{rc} is the transfer function for the rotor current controller. Combined, the DFIG with the rotor-side converter can be modeled as the circuit in Fig. 1. The current reference i_r^* acts as an equivalent current source, and the controller Z_{rc} as an impedance. R_s and R_r are usually negligible compared to Z_{rc} and therefore not shown in the circuit.

Neglecting the voltage drop on R_r, the rotor voltage v_r equals the EMF E_r. E_r can be decomposed into two parts:

$$E_r = E_{rm} + E_{ri} = -j\omega_r \psi_r + s\psi_r \tag{3}$$

in which $E_{rm} = -j\omega_r \psi_r$ is the motional EMF generated by the rotation of the rotor, and $E_{ri} = s\psi_r$ is the induced EMF generated by the variation of the flux (s represents the time derivative in the Laplace transform). As illustrated in Fig. 1, the motion-induction EMF composition forms an equivalent voltage amplifier (MIA) with the gain K determined by

$$K(s) = \frac{E_{ri}}{E_r} = \frac{s\psi_r}{-j\omega_r \psi_r + s\psi_r} = \frac{s}{s - j\omega_r}. \tag{4}$$

Across this amplifier the current i_r is unchanged, but the voltage (EMF) is amplified by K. As a result, the rotor controller impedance Z_{rc} is mapped to $Z_{rc}K$ seen from the other side of the amplifier. Letting $s = j\omega$, we get the frequency response of $K(s)$

$$K(j\omega) = \frac{\omega}{\omega - \omega_r}. \tag{5}$$

It is clear that $K(j\omega)$ is real-valued and < 0 for $\omega \in (0, \omega_r)$.

Now we turn to Z_{rc}, which is a proportional-integral (PI) controller in the synchronous frame and can be represented in the stationary frame as

$$Z_{rc} = k_p + \frac{k_i}{s - j\omega_g}. \tag{6}$$

in which k_p and k_i are the proportional and integral gain respectively, and ω_g is the grid synchronous frequency. The integrator $1/s$ is shifted to $1/(s - j\omega_g)$ due to frame transformation [32], [33].

Letting $s = j\omega$ again, we get the frequency response of Z_{rc}

$$Z_{rc}(j\omega) = k_p - j\frac{k_i}{\omega - \omega_g} \tag{7}$$

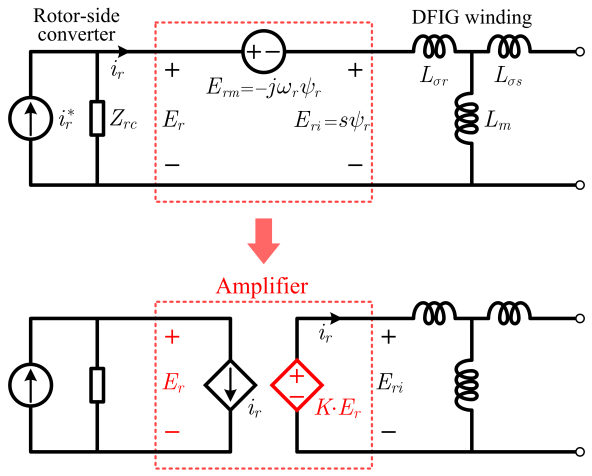

Fig. 1. Conceptual illustration of motion-induction amplification (MIA) effect: the combination of E_{rm} and E_{ri} forms an equivalent voltage amplifier.

and we see that the real part (resistance) of $Z_{rc}(j\omega)$ equals k_p and is always positive. Therefore, it is the MIA effect that gives rise to the negative resistance in $Z_{rc}K$, which is eventually propagated to the stator-side total impedance Z_s

$$Z_s = (Z_{rc}K + L_{\sigma r}s)||L_m s + L_{\sigma s}s. \tag{8}$$

The real parts of Z_{rc}, $Z_{rc}K$ and Z_s are plotted in Fig. 2 and compared with K to explicitly visualize the root cause of the negative resistance. Both the negative gain and the negative resistance appear in the frequency range $(0, \omega_r)$. ω_r usually varies within $(0.7\omega_g, 1.3\omega_g)$, and the LC resonant frequency ω_n is usually close to $0.5\omega_g$, which means that the resonant frequency coincides with the frequency range of negative resistance. This result agrees with [13] in which the effect of outer control loops are included. Negative resistance appears in the same frequency range as in [13], which confirms that the inner-loop model in this paper preserves the key characteristics of negative damping related to SSO.

It is worth noting that the MIA concept yields the same result as the induction generator effect. The MIA gain actually

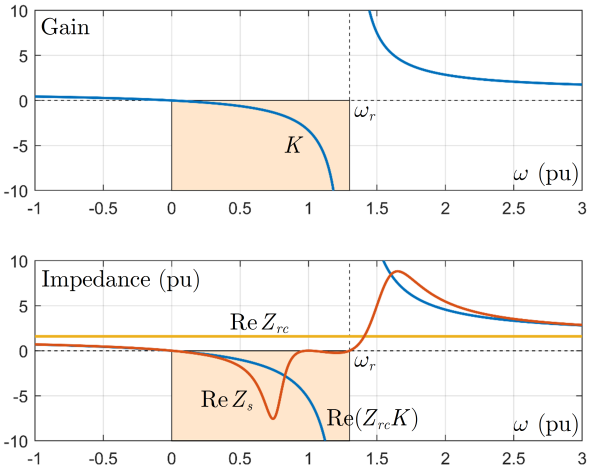

Fig. 2. Frequency response of K and the real parts of Z_{rc}, $Z_{rc}K$, and Z_s.

equals the reciprocal of slip in the frequency domain, that is, $K(j\omega) = 1/S(\omega)$ where $S(\omega) = 1 - \omega_r/\omega$ denotes the slip as a function of frequency [14]. However, the MIA interpretation preserves the internal structure of rotor EMF which is invisible in slip itself, and offers more insight in to the physical root cause of SSO. The rotational EMF absorbs mechanical energy from the shaft and converts it to electrical energy. This energy injection induces voltage amplification and negative resistance, which excites the LC resonance. In the light of this insight, the SSO can be eliminated if the injected energy is re-directed back to the rotor-side converter. Following this idea, we can design converter control schemes to counteract the MIA and thereby eliminate the negative resistance of a DFIG, as described in the succeeding section.

III. Motion-Induction Compensation

The MIA effect not only explains the root cause of DFIG negative resistance, but also sheds light on methods of mitigation. Compensation control can be embedded in the rotor-side converter to cancel the the effect of MIA and thereby eliminate the negative resistance. This method is called motion-induction compensation (MIC) to highlight its link with MIA. Two MIC techniques, namely additive and multiplicative MIC, are proposed and explained below.

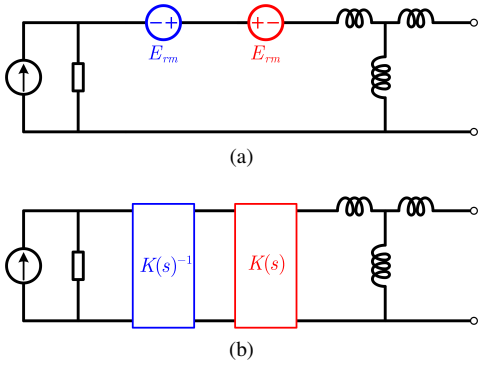

Fig. 3. The concept of motion-induction compensation (MIC). (a) Additive MIC. (b) Multiplicative MIC.

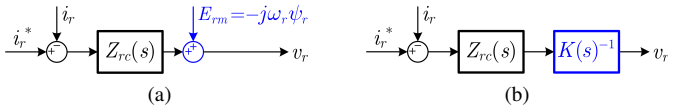

Fig. 4. The control algorithms for motion-induction compensation (MIC). (a) Additive MIC. (b) Multiplicative MIC.

A. Additive Compensation

In the additive compensation, a virtual voltage source of opposite direction is added to cancel the motional EMF E_{rm} seen from Z_{rc}, as shown in Fig. 3 (a). This virtual voltage source can be realized by adding an extra signal on the output of the rotor current controller Z_{rc}, as shown in Fig. 4 (a). Two variables are used in this compensation, namely rotor frequency ω_r and rotor flux linkage ψ_r. ω_r is directly measured in most wind turbines; ψ_r is not measured but can

be estimated from voltage and current. There are various flux linkage estimation algorithms and we choose to used current based estimation based on the flux equation in (1).

B. Multiplicative Compensation

An alternative method to cancel MIA is to embed an inverse system K^{-1} in the controller so that $K^{-1}\cdot K = 1$, as shown in Fig. 3 (b). This inverse system can be realized by multiplying K^{-1} on the original current controller Z_{rc}, as shown in Fig. 4 (b). Using (4), we have

$$K^{-1}(s) = \frac{s - j\omega_r}{s} = 1 - \frac{j\omega_r}{s}. \tag{9}$$

This $K^{-1}(s)$ is represented in the stationary frame, and we can transform it to the synchronous frame (dq) by substituting s with $s + j\omega_g$

$$K_{dq}^{-1}(s) = K^{-1}(s + j\omega_g) = 1 - \frac{j\omega_r}{s + j\omega_g}. \tag{10}$$

in which ω_g can be updated in real time from a phase-locked loop. Compared to the additive compensation, the multiplicative compensation does not need flux estimation, but changes the loop structure of the rotor current control.

C. Feed-forward decoupling

Feed-forward decoupling is commonly used in inverter control to decouple the dynamic response of active and reactive currents. In this subsection, we investigate the decoupling schemes with MIC. We transform the state equation in (1) to the synchronous frame as this is where the decoupling takes effect

$$\begin{aligned} \dot{\psi}_s &= v_s - j\omega_g\psi_s \\ \dot{\psi}_r &= v_r - j(\omega_g - \omega_r)\psi_r \end{aligned}. \tag{11}$$

The resistances R_s and R_r are neglected here. Changing the state variables from (ψ_s, ψ_r) to (ψ_s, i_r), we get

$$\begin{aligned} \dot{\psi}_s &= v_s - j\omega_g\psi_s \\ L_\sigma\dot{i}_r &= v_r - j(\omega_g - \omega_r)L_\sigma i_r + \tfrac{L_m}{L_s}j\omega_r\psi_s - \tfrac{L_m}{L_s}v_s \end{aligned} \tag{12}$$

in which $L_\sigma = (L_sL_r - L_m^2)/L_s$, $L_s = L_{\sigma s} + L_m$, and $L_r = L_{\sigma r} + L_m$.

If the DFIG is connected to an ideal grid, v_s is constant in the synchronous frame, and so is ψ_s since ψ_s is completely determined by v_s. For a non-ideal grid, the grid inductance can be counted into the leakage inductance of the DFIG, such that the conclusion above still hold. As a result, the current dynamics in (12) becomes

$$L_\sigma\dot{i}_r = v_r - j(\omega_g - \omega_r)L_\sigma i_r + \text{constant}. \tag{13}$$

It is clear that the only cross-coupling item is $j(\omega_g - \omega_r)L_\sigma i_r$, as the complex coefficient maps across the d and q axis, that is, $j\cdot(i_{rd} + ji_{rq}) = -i_{rq} + ji_{rd}$. This cross-coupling can be eliminated by adding a counteracting item in the rotor current controller

$$v_r = Z_{rc}\cdot(i_r^* - i_r) + j(\omega_g - \omega_r)L_\sigma i_r \tag{14}$$

which gives the commonly used feed-forward decoupling control [34].

If MIC is added in the rotor controller, the decoupling scheme above no longer holds since it overlaps with MIC itself. To show this, we change the state variable to (ψ_r, i_r) and rewrite (12) as

$$\begin{aligned} \dot{\psi}_r &= v_r - j(\omega_g - \omega_r)\psi_r \\ L_\sigma\dot{i}_r &= v_r - j\omega_g L_\sigma i_r + j\omega_r\psi_r - \tfrac{L_m}{L_s}v_s \end{aligned}. \tag{15}$$

v_s is still assumed constant, and $j\omega_r\psi_r$ is canceled by the MIC control (explicitly in the additive MIC, and implicitly in the multiplicative MIC). Therefore, the coupling item is $j\omega_g L_\sigma i_r$, and we get the decoupling scheme with MIC, as shown in Fig. 5. Compared to (14), this decoupling scheme is independent of ω_r because motional EMF is already compensated in the MIC. It is also worth noting that the decoupling scheme is invariant under frame transformation and therefore can be implemented in an arbitrary frame although it is derived here in the synchronous frame. The effect of the decoupling control is equivalent to a simple virtual reactance $-j\omega_g L_\sigma$, as shown in Fig. 6.

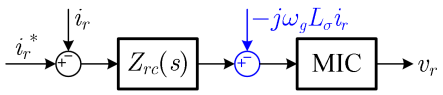

Fig. 5. Feed-forward decoupling control with MIC.

D. Passivity Based Interpretation

The equivalent circuit of the DFIG with MIC and decoupling control is shown in Fig. 6. MIA and MIC in the dashed blocks cancel each other. The decoupling control acts as a virtual reactance $-j\omega_g L_\sigma$ in series with the leakage winding inductance. The current controller acts as a virtual impedance Z_{rc} in parallel with the current source i_r^*. The virtual reactance ($-j\omega_g L_\sigma$), virtual impedance (Z_{rc}), winding inductance ($L_{\sigma r}$, $L_{\sigma s}$, L_m) and the series-compensated transmission line are all passive elements, so the entire circuit is a passive system which by itself ensures stability according to the passivity based control theory [35]. To illustrate this passivation effect of MIC, we draw the total stator-side impedance (Z_s) of a DFIG in Fig. 7, and it is seen that with MIC the impedance curve is constrained within the right half plane and the negative resistance is eliminated across the entire frequency range. This further confirms the small-signal passivity of a DFIG with

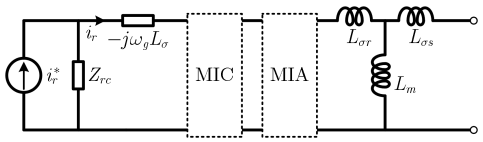

Fig. 6. Equivalent circuit for DFIG with MIC and feed-forward decoupling control: current-controlled inverter behind inductance. MIC cancels MIA. Feed-forward decoupling acts as a virtual reactance $-j\omega_g L_\sigma$ in series with the leakage inductance.

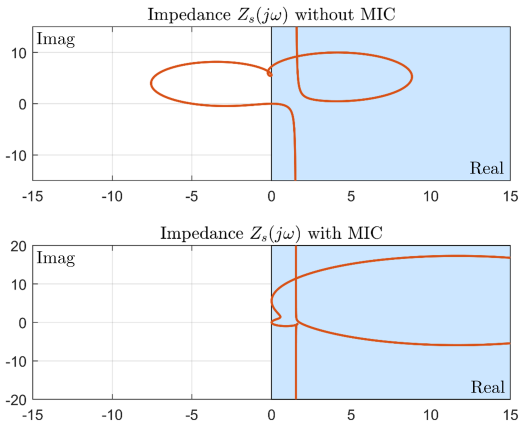

Fig. 7. DFIG impedance Z_s seen from the stator with and without MIC: MIC has a passivation effect and ensure positive real part (resistance) in the entire frequency range.

MIC control [36]. In fact, the MIC cancels the intrinsic dynamics of the DFIG and makes the Type-III generator behave like a Type-IV generator. That is, the generator is dynamically decoupled to the grid and presents itself as a simple current-controlled inverter behind inductance. As a result, the MIC not only achieves passivity but also preserves the current control performance (current tracking and decoupling).

IV. Model and Measurement Error Robustness

MIC provides theoretically guaranteed elimination of negative resistance and therefore offers very robust SSO damping that is independent of the parameters of the series-compensated line. However, MIC is still dependent upon the parameters of the DFIG model and local feedback measurements. The errors in the model and measurements may result in imperfect MIC and undermine its effect of SSO damping. This section provides a quantitative analysis on the error tolerance of MIC control to further confirm its robustness in practical application.

For the additive MIC, there are two sources of error, namely ω_r and ψ_r. We use the notation $x' = x + \Delta x$ to represent the error Δx between the real value x and modeled/measured value x', which gives the following derivation

$$\begin{aligned} &j\omega_r'\psi_r' \\ =&j(\omega_r+\Delta\omega_r)\big((L_m+\Delta L_m)(i_s+i_r)+(L_{\sigma r}+\Delta L_{\sigma r})i_r\big) \\ =&j\omega_r\psi_r + j\alpha\omega_r\psi_r + j\beta\omega_r L_{\sigma r} i_r \end{aligned} \tag{16}$$

in which

$$\alpha = \frac{\Delta\omega_r}{\omega_r} + \frac{\Delta L_m}{L_m} + \frac{\Delta\omega_r \Delta L_m}{\omega_r L_m} \tag{17}$$

and

$$\beta = \left(1+\frac{\Delta\omega_r}{\omega_r}\right)\left(\frac{\Delta L_{\sigma r}}{L_{\sigma r}} - \frac{\Delta L_m}{L_m}\right). \tag{18}$$

The flux linkage ψ_r' is estimated from current and inductance according to (1), and the current measurement error is counted into inductance error.

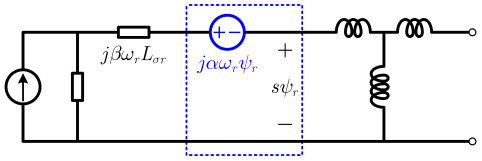

Fig. 8. The effect of model and measurement error in additive MIC.

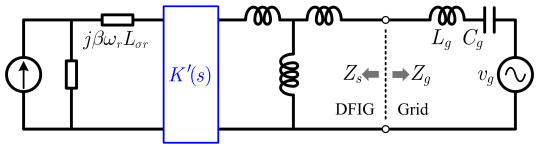

Fig. 9. Closed-loop system of DFIG (with additive MIC) connected to series-compensated line.

When using $j\omega_r'\psi_r'$ for MIC, the MIA effect is only partly canceled, and a residual error $j\alpha\omega_r\psi_r + j\beta\omega_r L_{\sigma r} i_r$ is induced. The effect of this error is clearly seen in the equivalent circuit in Fig. 8. The second item $j\beta\omega_r L_{\sigma r} i_r$ acts as a reactance, and the first item $j\alpha\omega_r\psi_r$ forms a new amplifier together with $s\psi_r$

$$K'(s) = \frac{s\psi_r}{s\psi_r + j\alpha\omega_r\psi_r} = \frac{s}{s+j\alpha\omega_r}. \tag{19}$$

We name $K'(s)$ a *residual amplifier* as it is the leftover of incomplete cancellation of MIA. Again, letting $s = j\omega$, we get

$$K'(j\omega) = \frac{\omega}{\omega + \alpha\omega_r}. \tag{20}$$

If $\alpha = 0$, $K' = 1$ meaning the MIA is fully canceled. If $\alpha \neq 0$, K' is negative for ω between 0 and $-\alpha\omega_r$. The smaller α is, the narrower is the frequency range of negative gain.

We now give an estimation of α and β. The measurement of ω_r comes from speed sensors and is usually very accurate, but the parameters of L_m and $L_{\sigma r}$ may have higher errors due to the variation of the air gap and magnetization curve. Assuming

$$\frac{\Delta\omega_r}{\omega_r} = \pm 1\%,\ \frac{\Delta L_m}{L_m} = \pm 10\%,\ \frac{\Delta L_{\sigma r}}{L_{\sigma r}} = \pm 10\% \tag{21}$$

we have

$$\alpha \approx \pm 11\%,\ \beta \approx \pm 20\%. \tag{22}$$

With these typical errors, $|\alpha\omega_r|$ is much smaller than the resonant frequency ω_n, implying that the negative resistance does not overlap with the resonance in frequency so the SSO will not be excited.

As the DFIG is no longer passive for $\alpha \neq 0$, we have to turn to the Nyquist criterion for a rigorous evaluation of stability, which is presented below. The closed-loop system of a DFIG connected to a series-compensated grid is shown in Fig. 9, whose stability is determined by the magnitude and phase relationship of the DFIG impedance (Z_s) and grid impedance (Z_g) according to Nyquist criterion [37]. Z_s here includes the effects of rotor current controller, MIC, MIA, as well as the winding resistances R_s and R_r. The grid is represented in Thevenin's form with an infinite source behind Z_g. The mechanical dynamics of the grid is not included in the model as we assume that the grid inertia is high enough to

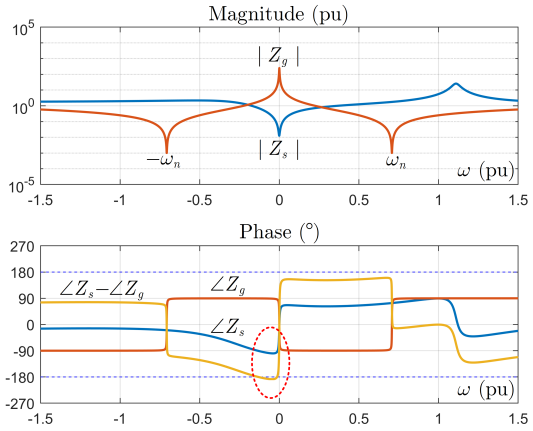

(a)

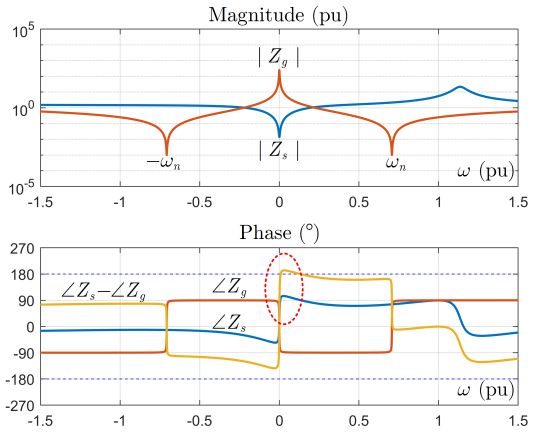

(b)

Fig. 10. Bode plot of Z_s and Z_g under additive MIC control. (a) $\alpha = 11\%$. (b) $\alpha = -11\%$.

be considered infinite in SSO analysis. Gas-turbine generators with sub-synchronous torsional dynamics may participate in SSO [9], but this is beyond the scope of this paper. As shown in the Bode plots in Fig. 10, the phase difference $\angle Z_s - \angle Z_g$ exceeds $\pm 180°$ between 0 and $-\alpha\omega_r$ (highlighted in the dashed circle), but this does not result in instability since $|Z_s/Z_g| < 1$ (because $|Z_s| < |Z_g|$) in this range so the Nyquist curve of Z_s/Z_g does not encircle the $(-1, 0)$ point. Therefore, it can be concluded that the additive MIC has a good tolerance against model and measurement errors.

The analysis of error tolerance for multiplicative MIC is similar. The multiplicative MIC is sensitive to ω_r, and an imperfect measurement on ω_r results in a residual amplifier $K''(s)$ as shown in Fig. 11:

$$K''(s) = \frac{s - j\omega_r - j\Delta\omega_r}{s - j\omega_r} \tag{23}$$

and

$$K''(j\omega) = \frac{\omega - \omega_r - \Delta\omega_r}{\omega - \omega_r} \tag{24}$$

in which $\Delta\omega_r$ is the error on ω_r and $\Delta\omega_r = \pm 1\%\omega_r$ as explained previously. K'' is negative for ω between ω_r and $\omega_r + \Delta\omega_r$, which may cause instability. We again use a Bode plot and the Nyquist criterion to evaluate stability, but change the splitting point of impedance to the rotor side as in Fig. 11. The Bode plot in Fig. 12 (a) reveals that K'' causes resonance around ω_r making the system unstable.

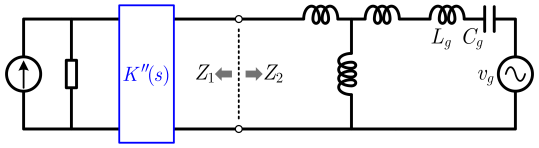

Fig. 11. Error tolerance analysis on multiplicative MIC.

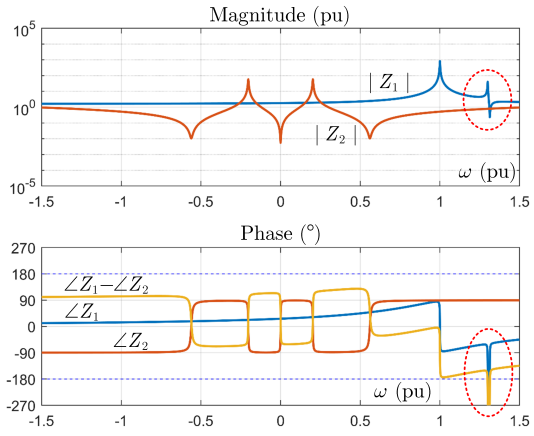

(a)

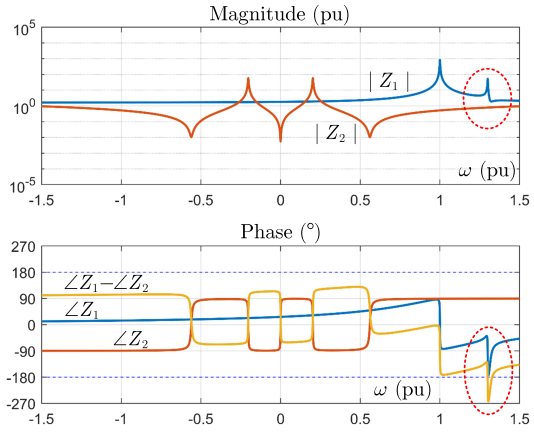

(b)

Fig. 12. Bode plot of Z_1 and Z_2 under multiplicative MIC control. (a) Without damping. (b) With damping.

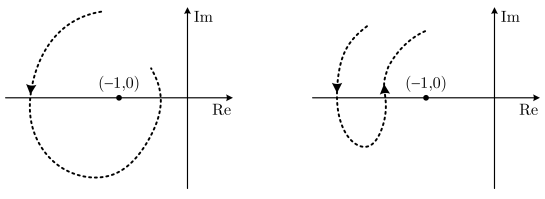

(a) (b)

Fig. 13. Nyquist curve of Z_1/Z_2 under multiplicative MIC control. (a) Without damping: encircling $(-1, 0)$. (b) With damping: not encircling.

This problem can be solved by adding damping in the multiplicative MIC. The damped MIC is defined as

$$K_d^{-1}(s) = \frac{s - j\omega_r + \sigma}{s} = 1 - \frac{j\omega_r - \sigma}{s} \tag{25}$$

and the corresponding residual amplifier is

$$K_d''(s) = \frac{s - j\omega_r - j\Delta\omega_r + \sigma}{s - j\omega_r}. \tag{26}$$

in which σ is the damping parameter.

After adding damping, the resonance near ω_r in Z_1 is clipped and the system becomes stable, as shown in Fig. 12 (b). It is noted that in both cases (with and without damping), the phase difference $\angle Z_s - \angle Z_g$ goes beyond $-180°$, but when damping is added, the phase of Z_1/Z_2 comes back to $> -180°$ before encircling the $(-1, 0)$ point, as illustrated in Fig. 13, implying that the system is stabilized. As a result, both the additive and multiplicative MIC can be designed to have very high robustness against model and measurement errors.

V. Simulation Verification

The effectiveness of the proposed MIC methods in SSO damping is verified with simulation tests. The configuration of the simulated system is displayed in Fig. 14. The wind farm contains 100×1.5MW Type-III (DFIG) wind turbines, which are represented by a single aggregated model. The wind generators are connected by collector networks and fed into a series-compensated transmission line. A bypass switch is used to control the series capacitor. The reactance of the series capacitor X_S is a fraction of the transmission line reactance X_L, that is, $X_S = k_S X_L$, in which k_S is the series compensation ratio. Two typical values of $k_S = 50\%,\ 75\%$ are used in this case study. The standard grid-voltage-oriented control [27] is used for DFIG and all inner and outer control loops are preserved to ensure fidelity. The PI control in the RSC current loop is replaced by PI+MIC control to test the effect of the proposed MIC in SSO damping, as shown in Fig. 15. The converters are represented by averaged switching models to speed-up the simulation, but discrete-time control is used to include the effect of digital control and modulation delay. The parameters of the DFIGs and the converters are listed in Table I.

Fig. 16 shows the comparison of the damping of SSO by two baseline solutions and the two proposed MIC approaches. In these tests, the series capacitor is inserted into the transmission line at time = 0.1s to initiate the SSO behavior. The measured stator-side active/reactive power ($P_s,\ Q_s$) and grid voltage magnitude (V_m, measured at the point of common coupling) are displayed. A variety of cases (A, B, C, shown in different colors) with different rotor speeds (sub-synchronous $\omega_r = 0.7\omega_g$, super-synchronous $\omega_r = 1.3\omega_g$) and different compensation ratios ($k_S = 50\%$, $k_S = 75\%$) are tested. Two state-of-the-art SSO damping methods are selected as the baseline, namely reducing gain [16] and supplementary damping control [21]. Reducing gain has the worst damping performance among the compared results and is unstable for Case C. The supplementary damping control is tuned for the compensation ratio of $k_S = 75\%$ (Case A) and has comparable performance to the proposed MIC control for this particular case. However, its damping effect is compromised (Case B), and even becomes unstable (Case C) for $k_S = 50\%$ due to the mismatch between the series capacitor value and the assumed compensation. In contrast, the proposed MIC schemes (both additive and multiplicative) show superior damping performances in all the tested cases. These results demonstrate the clear advantage of MIC control in providing wide-range SSO damping that is insensitive to operating conditions.

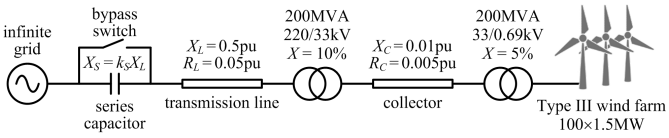

Fig. 14. Configuration of the simulated wind farm.

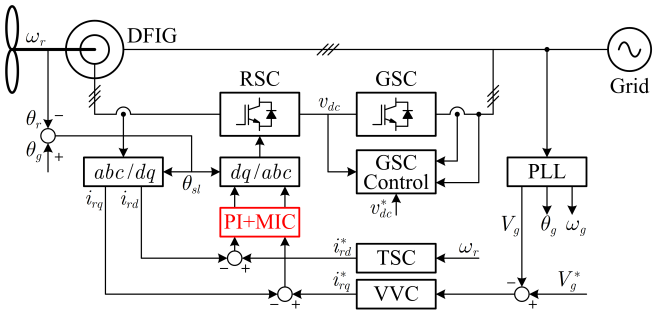

Fig. 15. DFIG control scheme used in the simulation. The RSC current loop uses PI+MIC instead of PI control. The phase-locked loop (PLL) observes the amplitude, phase and frequency of grid voltage (V_g, θ_g, and ω_g). The torque-speed control (TSC) governs the RSC active current reference (i_d^*). The voltage-var control (VVC) governs the RSC reactive current reference (i_q^*).

TABLE I
Parameters of the Simulated DFIGs and Converters.

Stator nominal voltage	0.69kV	DC link voltage	1.4kV
Stator/rotor turn ratio	3:10	Nominal slip	±0.3
Stator leakage inductance	0.17pu	Stator resistance	0.0084pu
Rotor leakage inductance	0.13pu	Rotor resistance	0.0083pu
Mutual inductance	5.42pu	DC link capacitor	30mF
Switching frequency	1kHz	Sampling frequency	2kHz

Fig. 17 shows the step response of rotor currents to test the current tracking performance of MIC control. Under the step change of i_{rd}^* (d-axis current reference, proportional to shaft torque), the rising time of the responding rotor currents i_{rd} and i_{rq} is less than 20ms and the settling time is less than 100ms. The current tracking waveform is comparable to the conventional PI control in a non-compensated grid (which is not stable in a series-compensated grid), meaning that the MIC control mitigates the SSO without compromising the tracking performance. It is also clear from the comparison that the decoupling control effectively mitigate the cross-coupling of i_{rd} and i_{rq}, resulting in nearly independent dynamic response.

Fig. 18 tests the robustness of the proposed MIC control under model and measurement errors ($1\%\omega_r,\ 10\%L_m$). The

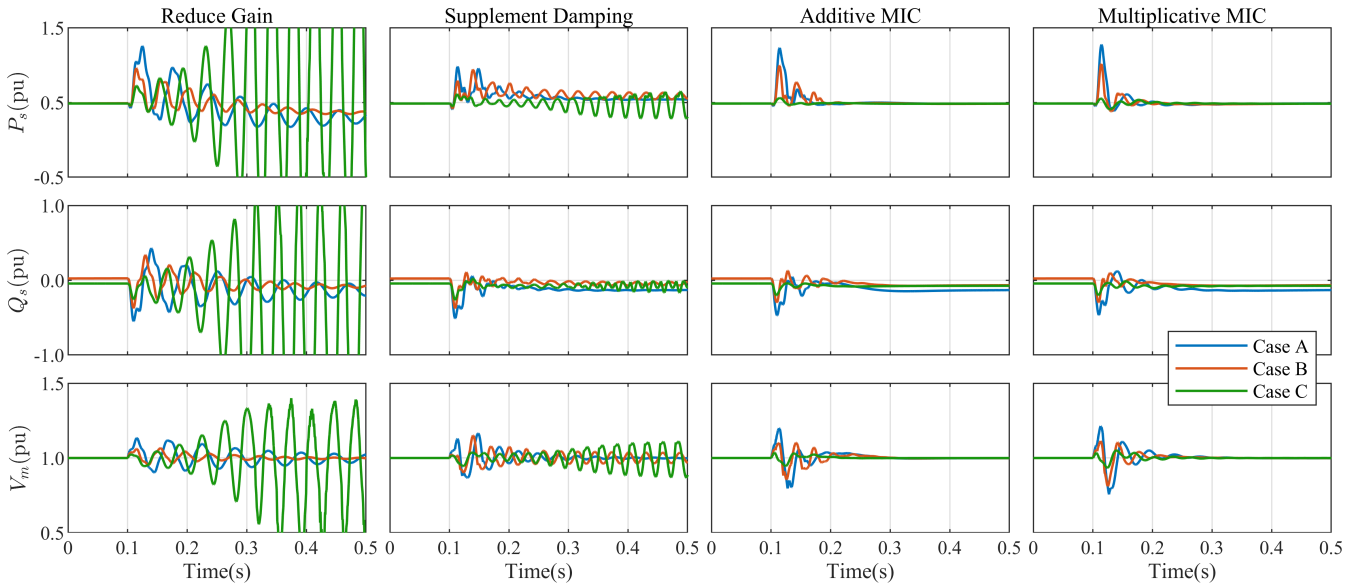

Fig. 16. Capacitor insertion responses under different control schemes (represented by columns) in different cases (represented by colors). Case A: 75% compensation, $\omega_r = 1.3\omega_g$; Case B: 50% compensation, $\omega_r = 1.3\omega_g$; Case C: 50% compensation, $\omega_r = 0.7\omega_g$.

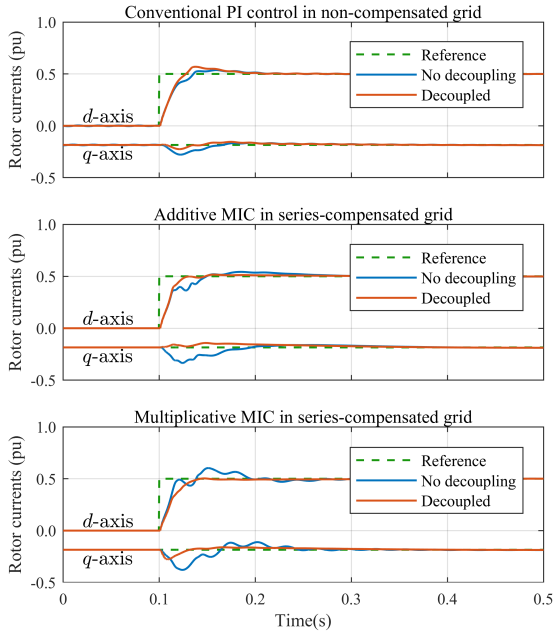

Fig. 17. Step responses show good current tracking of MIC control.

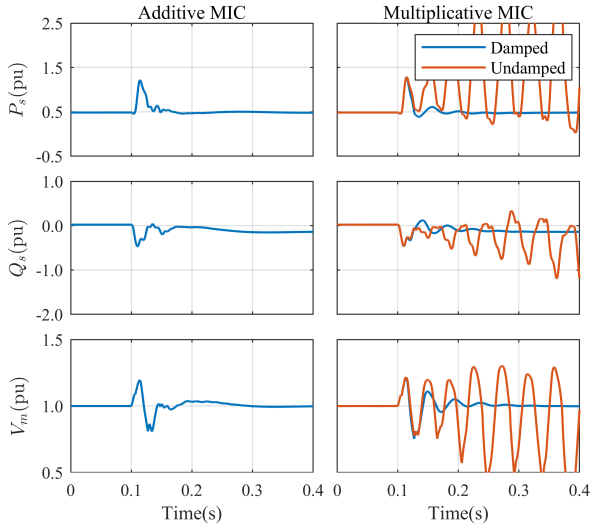

Fig. 18. Capacitor insertion responses with measurement and parameter error showing good robustness.

test results show that the additive MIC is immune against these errors by itself. The multiplicative MIC is not as robust, but can retain the robustness via adding extra damping in the controller as described in section IV.

VI. Conclusions

A novel DFIG SSO damping control scheme called motion-induction compensation (MIC) has been proposed based on the concept of motion-induction amplification (MIA). This MIC control makes a Type-III generator (DFIG) behave like a Type-IV generator and thereby eliminates the negative resistance otherwise present in a DFIG in the sub-synchronous frequency range. As a result, the MIC control ensures effective (positive) SSO damping that is independent of the configuration of series-compensated lines in the wider transmission network. Theoretical analysis shows that MIC has very good robustness against model and measurement errors. Simulation tests demonstrate clear advantages of the proposed method over the state-of-the-art solutions in providing robust SSO damping in a wide range of operating conditions.

References

[1] Siemens Gamesa reducing product line to cut costs, grow market share. [Online]. Available: http://www.hutchpost.com/siemens-gamesa-reducing-product-line-to-cut-costs-grow-market-share/?from=timeline

[2] Wind Turbine Overview, GE Renewable Energy. [Online]. Available: https://www.ge.com/renewableenergy/wind-energy/turbines

[3] K. Xiahou, X. Lin, Y. Liu, and Q. H. Wu, "Robust Rotor-Current Sensorless Control of Doubly Fed Induction Generators," *IEEE Trans. Energy Convers.*, vol. 33, no. 2, pp. 897–899, June 2018.

[4] J. Zhu, J. Hu, W. Hung, C. Wang, X. Zhang, S. Bu, Q. Li, H. Urdal, and C. D. Booth, "Synthetic Inertia Control Strategy for Doubly Fed Induction Generator Wind Turbine Generators Using Lithium-Ion Supercapacitors," *IEEE Trans. Energy Convers.*, vol. 33, no. 2, pp. 773–783, June 2018.

[5] J. Ying, X. Yuan, J. Hu, and W. He, "Impact of Inertia Control of DFIG-Based WT on Electromechanical Oscillation Damping of SG," *IEEE Trans. Power Syst.*, vol. 33, no. 3, pp. 3450–3459, May 2018.

[6] R. K. Varma, S. Auddy, and Y. Semsedini, "Mitigation of Subsynchronous Resonance in a Series-Compensated Wind Farm Using FACTS Controllers," *IEEE Trans. Power Del.*, vol. 23, no. 3, pp. 1645–1654, July 2008.

[7] A. Moharana, R. K. Varma, and R. Seethapathy, "SSR Alleviation by STATCOM in Induction-Generator-Based Wind Farm Connected to Series Compensated Line," *IEEE Trans. Sustain. Energy*, vol. 5, no. 3, pp. 947–957, July 2014.

[8] L. Piyasinghe, Z. Miao, J. Khazaei, and L. Fan, "Impedance Model-Based SSR Analysis for TCSC Compensated Type-3 Wind Energy Delivery Systems," *IEEE Trans. Sustain. Energy*, vol. 6, no. 1, pp. 179–187, Jan 2015.

[9] W. Du, Y. Wang, H. Wang, and Q. Fu, "Concept of Modal Repulsion for Examining the Sub-Synchronous Oscillations in Power Systems," *IEEE Trans. Power Syst.*, vol. 33, no. 4, pp. 4614–4624, July 2018.

[10] J. Adams, C. Carter, and S.-H. Huang, "ERCOT experience with sub-synchronous control interaction and proposed remediation," in *Transmission and Distribution Conference and Exposition (T&D), 2012 IEEE PES*. IEEE, 2012, pp. 1–5.

[11] K. Narendra, D. Fedirchuk, R. Midence, N. Zhang, A. Mulawarman, P. Mysore, and V. Sood, "New microprocessor based relay to monitor and protect power systems against sub-harmonics," in *2011 IEEE Electrical Power and Energy Conference*, Oct 2011, pp. 438–443.

[12] P. Kundur, N. J. Balu, and M. G. Lauby, *Power system stability and control*. McGraw-hill New York, 1994, vol. 7.

[13] I. Vieto and J. Sun, "Sequence Impedance Modeling and Analysis of Type-III Wind Turbines," *IEEE Trans. Energy Convers.*, vol. 33, no. 2, pp. 537–545, June 2018.

[14] L. Fan and Z. Miao, "Nyquist-Stability-Criterion-Based SSR Explanation for Type-3 Wind Generators," *IEEE Trans. Energy Convers.*, vol. 27, no. 3, pp. 807–809, Sep. 2012.

[15] K. Gu, F. Wu, and X. Zhang, "Sub-synchronous interactions in power systems with wind turbines: a review," *IET Renewable Power Generation*, vol. 13, no. 1, pp. 4–15, 2019.

[16] W. Ren, E. V. Larsen, and S. A. Barker, "System and method for adjusting current regulator gains applied within a power generation system," Jan. 17 2017, US Patent 9,548,690.

[17] H. Liu, X. Xie, Y. Li, H. Liu, and Y. Hu, "Mitigation of SSR by embedding subsynchronous notch filters into DFIG converter controllers," *IET Generation, Transmission Distribution*, vol. 11, no. 11, pp. 2888–2896, 2017.

[18] A. E. Leon, "Integration of DFIG-Based Wind Farms Into Series-Compensated Transmission Systems," *IEEE Trans. Sustain. Energy*, vol. 7, no. 2, pp. 451–460, April 2016.

[19] L. Fan and Z. Miao, "Mitigating SSR Using DFIG-Based Wind Generation," *IEEE Trans. Sustain. Energy*, vol. 3, no. 3, pp. 349–358, July 2012.

[20] A. E. Leon and J. A. Solsona, "Sub-Synchronous Interaction Damping Control for DFIG Wind Turbines," *IEEE Trans. Power Syst.*, vol. 30, no. 1, pp. 419–428, Jan 2015.

[21] H. A. Mohammadpour and E. Santi, "SSR Damping Controller Design and Optimal Placement in Rotor-Side and Grid-Side Converters of Series-Compensated DFIG-Based Wind Farm," *IEEE Trans. Sustain. Energy*, vol. 6, no. 2, pp. 388–399, April 2015.

[22] P. Huang, M. S. El Moursi, W. Xiao, and J. L. Kirtley, "Subsynchronous Resonance Mitigation for Series-Compensated DFIG-Based Wind Farm by Using Two-Degree-of-Freedom Control Strategy," *IEEE Trans. Power Syst.*, vol. 30, no. 3, pp. 1442–1454, May 2015.

[23] L. Wang, X. Xie, Q. Jiang, H. Liu, Y. Li, and H. Liu, "Investigation of SSR in Practical DFIG-Based Wind Farms Connected to a Series-Compensated Power System," *IEEE Trans. Power Syst.*, vol. 30, no. 5, pp. 2772–2779, Sept 2015.

[24] S. Chernet, M. Bongiorno, G. K. Andersen, T. Lund, and P. C. Kjaer, "Online variation of wind turbine controller parameter for mitigation of SSR in DFIG based wind farms," in *2016 IEEE Energy Conversion Congress and Exposition (ECCE)*, Sept 2016, pp. 1–8.

[25] H. Liu, X. Xie, J. He, T. Xu, Z. Yu, C. Wang, and C. Zhang, "Subsynchronous Interaction Between Direct-Drive PMSG Based Wind Farms and Weak AC Networks," *IEEE Trans. Power Syst.*, vol. 32, no. 6, pp. 4708–4720, Nov 2017.

[26] L. Harnefors, X. Wang, A. G. Yepes, and F. Blaabjerg, "Passivity-Based Stability Assessment of Grid-Connected VSCs - An Overview," *IEEE Journal of Emerging and Selected Topics in Power Electronics*, vol. 4, no. 1, pp. 116–125, March 2016.

[27] B. Wu, Y. Lang, N. Zargari, and S. Kouro, *Power conversion and control of wind energy systems*. John Wiley & Sons, 2011, vol. 76.

[28] J. Holtz, "The representation of AC machine dynamics by complex signal flow graphs," *IEEE Trans. Ind. Electron.*, vol. 42, no. 3, pp. 263–271, Jun 1995.

[29] L. Harnefors, "Modeling of Three-Phase Dynamic Systems Using Complex Transfer Functions and Transfer Matrices," *IEEE Trans. Ind. Electron.*, vol. 54, no. 4, pp. 2239–2248, Aug 2007.

[30] Y. Gu, Y. Li, and T. C. Green, "Interpreting frame transformations as diagonalization of harmonic transfer functions," *arXiv preprint arXiv:1810.09911v4*, 2018.

[31] Y. Gu, N. Bottrell, and T. C. Green, "Reduced-order models for representing converters in power system studies," *IEEE Transactions on Power Electronics*, vol. 33, no. 4, pp. 3644–3654, 2017.

[32] J. Shen, S. Schrder, H. Stagge, and R. W. D. Doncker, "Precise modeling and analysis of DQ-frame current controller for high power converters with low pulse ratio," in *2012 IEEE Energy Conversion Congress and Exposition (ECCE)*, Sept 2012, pp. 61–68.

[33] D. N. Zmood and D. G. Holmes, "Stationary frame current regulation of PWM inverters with zero steady-state error," *IEEE Trans. Power Electron.*, vol. 18, no. 3, pp. 814–822, May 2003.

[34] K. Kerrouche, A. Mezouar, and K. Belgacem, "Decoupled Control of Doubly Fed Induction Generator by Vector Control for Wind Energy Conversion System," *Energy Procedia*, vol. 42, pp. 239 – 248, 2013, mediterranean Green Energy Forum 2013: Proceedings of an International Conference MGEF-13. [Online]. Available: http://www.sciencedirect.com/science/article/pii/S1876610213017268

[35] R. Ortega, J. A. L. Perez, P. J. Nicklasson, and H. J. Sira-Ramirez, *Passivity-based control of Euler-Lagrange systems: mechanical, electrical and electromechanical applications*. Springer Science & Business Media, 2013.

[36] Y. Gu, W. Li, and X. He, "Passivity-Based Control of DC Microgrid for Self-Disciplined Stabilization," *IEEE Trans. Power Syst.*, vol. 30, no. 5, pp. 2623–2632, Sept 2015.

[37] J. Sun, "Impedance-based stability criterion for grid-connected inverters," *IEEE Trans. Power Electron.*, vol. 26, no. 11, pp. 3075–3078, 2011.

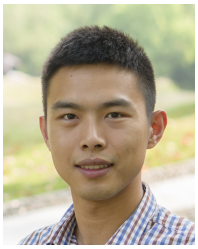

Yunjie Gu (M'18) received the B.Sc. and the Ph.D. degree in Electrical Engineering from Zhejiang University, Hangzhou, China, in 2010 and 2015 respectively. He was a Consulting Engineer at General Electric Global Research Centre, Shanghai, from 2015 to 2016, and is now an EPSRC-funded Innovation Fellow at Imperial College London (award EP/S000909/1). His research interests include power system control and stability, and the application of power electronics to power systems.

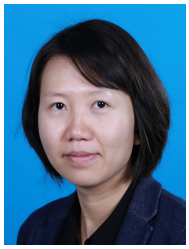

Jiao Liu Jiao Liu received the B.Sc and M.Sc degrees in Electrical Engineering from Zhejiang University, Hangzhou, China, in 2008 and 2011, respectively. From 2011 to 2017, she was a Research Engineer at General Electric Global Research Center, Shanghai, China. She is currently a Lead Engineer at GE Renewable Energy. Her research area is grid integration of renewable energy and power system stability.

Timothy C. Green (M'89-SM'02) received a B.Sc. (Eng) (first class honours) from Imperial College London, UK in 1986 and a Ph.D. from Heriot-Watt University, Edinburgh, UK in 1990. He is a Professor of Electrical Power Engineering at Imperial College London, and Director of the Energy Futures Lab with a role fostering interdisciplinary energy research. His research interest is in using the flexibility of power electronics to accommodate new generation patterns and new forms of load, such as EV charging, as part of the emerging smart grid. In HVDC he has contributed converter designs that reduce losses while also providing control functions assist AC system integration. In distribution systems, he has pioneered the use of soft open points and the study of stability of grid connected inverters. Prof. Green is a Chartered Engineering the UK and a Fellow of the Royal Academy of Engineering.

Wuhua Li (M09) received the B.Sc. and Ph.D. degree in Power Electronics and Electrical Engineering from Zhejiang University, Hangzhou, China, in 2002 and 2008, respectively. From 2004 to 2005, he was a Research Intern, and from 2007 to 2008, a Research Assistant in GE Global Research Center, Shanghai, China. From 2008 to 2010, he joined the College of Electrical Engineering, Zhejiang University as a Post doctor. In 2010, he was promoted as an Associate Professor. Since 2013, he has been a Full Professor at Zhejiang University. From 2010 to 2011, he was a Ryerson University Postdoctoral Fellow with the Department of Electrical and Computer Engineering, Ryerson University, Toronto, ON, Canada. His research interests include power devices, converter topologies and advanced controls for high power energy conversion systems. Dr. Li has published more than 200 peer-reviewed technical papers and holds over 30 issued/pending patents. Due to his excellent teaching and research contributions, Dr. Li received the 2012 Delta Young Scholar from Delta Environmental and Educational Foundation, the 2012 Outstanding Young Scholar from National Science Foundation of China (NSFC), the 2013 Chief Youth Scientist of National 973 Program, the 2014 Young Top-Notch Scholar of National Ten Thousand Talent Program. He serves as the Associated Editor of Journal of Emerging and Selected Topics in Power Electronics, IET Power Electronics, CSEE Journal of Power and Energy Systems, Proceedings of the Chinese Society for Electrical Engineering, Guest Editor of IET Renewable Power Generation for Special Issue DC and HVDC system technologies, Member of Editorial Board for Journal of Modern Power System and Clean Energy. He received one National Natural Science Award and four Scientific and Technological Achievement Awards from Zhejiang Provincial Government and the State Educational Ministry of China. He was appointed as the Most Cited Chinese Researchers by Elsevier since 2014.

Xiangning He (M95-SM96-F10) received the B.Sc. and M.Sc. degrees from Nanjing University of Aeronautical and Astronautical, Nanjing, China, in 1982 and 1985, respectively, and the Ph.D. degree from Zhejiang University, Hangzhou, China, in 1989. From 1985 to 1986, he was an Assistant Engineer at the 608 Institute of Aeronautical Industrial General Company, Zhuzhou, China. From 1989 to 1991, he was a Lecturer at Zhejiang University. In 1991, he obtained a Fellowship from the Royal Society of UK, and conducted research in the Department of Computing and Electrical Engineering, Heriot-Watt University, Edinburgh, UK, as a Post-Doctoral Research Fellow for two years. In 1994, he joined Zhejiang University as an Associate Professor. Since 1996, he has been a Full Professor in the College of Electrical Engineering, Zhejiang University. He was the Director of the Power Electronics Research Institute, the Head of the Department of Applied Electronics, the Vice Dean of the College of Electrical Engineering, and he is currently the Director of the National Specialty Laboratory for Power Electronics, Zhejiang University. His research interests are power electronics and their industrial applications. Dr. He is a Fellow of The Institute of Electrical and Electronics Engineers (IEEE) and was appointed as IEEE Distinguished Lecturer by the IEEE Power Electronics Society 2011–2015. He is also a Fellow of the Institution of Engineering and Technology (formerly IEE), UK.